



Stability of the boundary layer on a rotating disk for power-law fluids



P.T. Griffiths^{a,*}, S.O. Stephen^a, A.P. Bassom^b, S.J. Garrett^c

^aSchool of Mathematics, University of Birmingham, Edgbaston, Birmingham B15 2TT, UK

^bSchool of Mathematics & Statistics, The University of Western Australia, Crawley 6009, Australia

^cDepartment of Mathematics & Department of Engineering, University of Leicester, University Road, Leicester LE1 7RH, UK

ARTICLE INFO

Article history:

Received 29 October 2013

Received in revised form 20 February 2014

Accepted 24 February 2014

Available online 13 March 2014

Keywords:

Instability

Rotating disk flow

Power-law fluid

Crossflow vortices

ABSTRACT

The stability of the flow due to a rotating disk is considered for non-Newtonian fluids, specifically shear-thinning fluids that satisfy the power-law (Ostwald-de Waele) relationship. In this case the basic flow is not an exact solution of the Navier–Stokes equations, however, in the limit of large Reynolds number the flow inside the three-dimensional boundary layer can be determined via a similarity solution. An asymptotic analysis is presented in the limit of large Reynolds number. It is shown that the stationary spiral instabilities observed experimentally in the Newtonian case can be described for shear-thinning fluids by a linear stability analysis. Predictions for the wavenumber and wave angle of the disturbances suggest that shear-thinning fluids may have a stabilising effect on the flow.

© 2014 Elsevier B.V. All rights reserved.

1. Introduction

The stability of the boundary layer on a rotating disk due to the flow of a Newtonian fluid is a classical problem that has attracted a great deal of attention from numerous authors over many decades. The first theoretical investigation of this problem was performed by von Kármán [1]. The steady flow induced by the rotation of an infinite plane with uniform angular velocity is an exact solution of the Navier–Stokes equations. The flow is characterised by the lack of a radial pressure gradient near to the disk to balance the centrifugal forces, so the fluid spirals outwards. The disk acts as a centrifugal fan, the fluid emanating from the disk being replaced by an axial flow directed back towards the surface of the disk.

Batchelor [2] showed that this type of flow is in fact just a limiting case of a whole number of flows with similarity solutions in which both the infinite plane and the fluid at infinity rotate with differing angular velocities. The corresponding limiting case when the infinite plane is stationary and the fluid at infinity rotates at a constant angular velocity was first described by Bödeewadt [3].

The stability of the von Kármán flow was first investigated by Gregory et al. [4]. They observed spiral modes of instability in the form of co-rotating vortices, measuring the angle between the normal to the radius vector and the tangent to the vortices to be $\phi \approx 13^\circ$. Gregory et al. [4] showed that these experimental

observations were in excellent agreement with their own predictions obtained from a linear stability analysis. Hall [5] extended this work taking into account the viscous effects, showing that an additional stationary short-wavelength mode exists which has its structure fixed by a balance between viscous and Coriolis forces.

There have been several numerical studies of the stability of the von Kármán boundary layer. Examples include that of Malik [6], Lingwood [7]. Both studies used a parallel-flow approximation for the basic flow. Malik [6] considered convective instability and presented results for stationary vortices, finding that for a large Reynolds number $\phi \approx 13^\circ$ for inviscid neutrally stable modes. Lingwood [7] extended these results by considering Ekman and Bödeewadt flows. She also investigated the absolute instability of these flows, showing that the von Kármán boundary layer is locally absolutely unstable for Reynolds number above a critical value. Subsequently, Davies and Carpenter [8] considered the global behaviour of the absolute instability of the rotating-disk boundary layer. By direct numerical simulations of the linearised governing equations they were able to show that the local absolute instability does not produce a linear global instability. Suggesting that, instead, convective-type behaviour dominates, even within the region of local absolute instability.

Considerably less attention has been given to the problem of the boundary layer flow due to a rotating disk when considering a non-Newtonian fluid. Mitschka [9] extended the von Kármán solution to fluids that adhere to the power-law relationship. In this case the basic flow is not an exact solution of the Navier–Stokes equations and a boundary layer approximation is required. Both Mitschka and Ulbrecht [10], Andersson et al. [11] present

* Corresponding author. Tel.: +44 (0) 121 414 9051.

E-mail addresses: p.griffiths@pgr.bham.ac.uk (P.T. Griffiths), s.o.stephen@bham.ac.uk (S.O. Stephen), andrew.bassom@uwa.edu.au (A.P. Bassom), stephen.garrett@le.ac.uk (S.J. Garrett).

numerical solutions for the basic flow for shear-thickening and shear-thinning fluids. However, both sets of authors overlooked the importance of matching this boundary-layer flow with the outer flow. Denier and Hewitt [12] addressed this problem and presented corrected similarity solutions of the boundary-layer equations. This involved a comprehensive knowledge of the far-field behaviour. Their analysis revealed different situations for shear-thinning and shear-thickening fluids. For shear-thickening fluids the boundary-layer solution is complicated by a region of zero viscosity away from the boundary. For the more common shear-thinning fluids, beyond a critical level of shear-thinning, the basic flow solution grows in the far field, so it cannot be matched to an external flow. For more details of these cases the reader is referred to Denier and Hewitt [12].

Thus, in the current paper we restrict our attention to moderate levels of shear-thinning, where the boundary-layer solution may be matched to an outer flow (although this will not be in similarity form). In this case we can use a boundary-layer similarity solution to give an analytic description of the stability of the three-dimensional flow for large Reynolds numbers. This only requires knowledge of the boundary layer since this is where the vortices are confined.

Specifically, we look to extend the previous works concerning convective instability of Newtonian flows to include the additional viscous effects of a power-law fluid. The current study will follow the approach of Hall [5] to investigate the so called stationary “inviscid instabilities” with vortices occurring at the location of an inflection point of the effective velocity profile.

2. Formulation

Consider the flow of a steady incompressible non-Newtonian fluid due to a rotating disk located at $z = 0$. The disk rotates about the z -axis with angular velocity Ω . Working in a reference frame that rotates with the disk, the dimensionless continuity and Navier–Stokes equations are expressed as

$$\nabla \cdot \mathbf{u} = 0, \quad (1)$$

$$\mathbf{u} \cdot \nabla \mathbf{u} + 2[(\hat{\mathbf{z}} \times \mathbf{u}) - r\hat{\mathbf{r}}] = -\nabla p + \frac{1}{Re} \nabla \cdot \boldsymbol{\tau}. \quad (2)$$

Here $\mathbf{u} = (u, v, w)$ are the velocity components in cylindrical polar coordinates (r, θ, z) where r and z have been made dimensionless with respect to some reference length l and $(\hat{\mathbf{r}}, \hat{\boldsymbol{\theta}}, \hat{\mathbf{z}})$ are the corresponding unit vectors in the respective coordinate directions. The velocities and pressure have been non-dimensionalised by Ωl and $\rho \Omega^2 l^2$ respectively, the fluid density is ρ and p is the fluid pressure. The stress tensor $\boldsymbol{\tau}$ for incompressible non-Newtonian fluids is given by the generalised Newtonian model

$$\boldsymbol{\tau} = \mu \dot{\boldsymbol{\gamma}} \quad \text{with} \quad \mu = \mu(\dot{\boldsymbol{\gamma}}), \quad (3)$$

where $\dot{\boldsymbol{\gamma}} = \nabla \mathbf{u} + (\nabla \mathbf{u})^T$ is the rate of strain tensor and $\mu(\dot{\boldsymbol{\gamma}})$ is the non-Newtonian viscosity. The magnitude of the rate of strain tensor is

$$\dot{\boldsymbol{\gamma}} = \sqrt{\frac{\dot{\boldsymbol{\gamma}} : \dot{\boldsymbol{\gamma}}}{2}}. \quad (4)$$

The governing relationship for $\mu(\dot{\boldsymbol{\gamma}})$ when considering a power-law fluid is

$$\mu(\dot{\boldsymbol{\gamma}}) = m(\dot{\boldsymbol{\gamma}})^{n-1}, \quad (5)$$

where m is known as the consistency coefficient and n the power-law index, with $n > 1$, $n < 1$ corresponding to shear-thickening and shear-thinning fluids, respectively. The modified non-Newtonian Reynolds number is defined as $Re = \rho \Omega^2 l^2 / m$.

In the Newtonian case an exact solution of the Navier–Stokes equations exists, as was first determined by von Kármán [1]. Due

to the relative complexity of the modified stress tensor no such solution exists when considering the flow of a power-law fluid. However, in the limit of large Reynolds number progress can be made as the leading order boundary-layer equations admit a similarity solution analogous to the exact solution obtained in the Newtonian problem.

As noted by Denier and Hewitt [12] the boundary-layer equations at lowest order are

$$\frac{1}{r} \frac{\partial}{\partial r}(ru_B) + \frac{\partial w_B}{\partial z} = 0, \quad (6a)$$

$$u_B \frac{\partial u_B}{\partial r} + w_B \frac{\partial u_B}{\partial z} - \frac{(v_B + r)^2}{r} = \frac{1}{Re} \frac{\partial}{\partial z} \left(\mu_B \frac{\partial u_B}{\partial z} \right), \quad (6b)$$

$$u_B \frac{\partial v_B}{\partial r} + w_B \frac{\partial v_B}{\partial z} + \frac{u_B v_B}{r} + 2u_B = \frac{1}{Re} \frac{\partial}{\partial z} \left(\mu_B \frac{\partial v_B}{\partial z} \right), \quad (6c)$$

where

$$\mu_B = \left[\left(\frac{\partial u_B}{\partial z} \right)^2 + \left(\frac{\partial v_B}{\partial z} \right)^2 \right]^{(n-1)/2}. \quad (6d)$$

To solve for the basic flow inside the boundary layer Mitschka [9] introduced a similarity solution of the form

$$\mathbf{u}_B = [r\bar{u}(\eta), r\bar{v}(\eta), r^{(n-1)/(n+1)} Re^{-1/(n+1)} \bar{w}(\eta)], \quad (7)$$

where the similarity variable η is given by

$$\eta = r^{(1-n)/(n+1)} Re^{1/(n+1)} z. \quad (8)$$

The dimensionless functions \bar{u} , \bar{v} and \bar{w} are determined, after substitution of (7) into (6a)–(6c) and (6d) by

$$2\bar{u} + \frac{1-n}{n+1} \eta \bar{u}' + \bar{w}' = 0, \quad (9a)$$

$$\bar{u}^2 - (\bar{v} + 1)^2 + \left(\bar{w} + \frac{1-n}{n+1} \eta \bar{u} \right) \bar{u}' - [(\bar{u}^2 + \bar{v}^2)^{(n-1)/2} \bar{u}']' = 0, \quad (9b)$$

$$2\bar{u}(\bar{v} + 1) + \left(\bar{w} + \frac{1-n}{n+1} \eta \bar{u} \right) \bar{v}' - [(\bar{u}^2 + \bar{v}^2)^{(n-1)/2} \bar{v}']' = 0, \quad (9c)$$

where the primes denote differentiation with respect to η . The appropriate boundary conditions are

$$\bar{u} = \bar{v} = \bar{w} = 0 \quad \text{at} \quad \eta = 0, \quad (10a)$$

$$\bar{u} \rightarrow 0, \quad \bar{v} \rightarrow -1 \quad \text{as} \quad \eta \rightarrow \infty. \quad (10b)$$

Denier and Hewitt [12] have shown that bounded solutions to 9a, 9b and 9c subject to (10a) and (10b) exist only in the shear-thinning case for $n > \frac{1}{2}$. In the shear-thickening case they have shown that solutions become non-differentiable at some critical location η_c , and although it transpires that this singularity can be regularised entirely within the context of the power-law model, we will not consider such flows here. Thus in this study we will consider flows with power-law index in the range $\frac{1}{2} < n \leq 1$. They have also shown that for $\frac{1}{2} < n < 1$ to ensure the correct algebraic decay in the numerical solutions one must apply the Robin condition

$$(\bar{u}', \bar{v}') = \frac{n}{\eta(n-1)} (\bar{u}, \bar{v}) \quad \text{as} \quad \eta \rightarrow \infty, \quad (11)$$

at some suitably large value of $\eta = \eta_\infty \gg 1$. In the Newtonian case this relationship becomes singular, this is due to the fact that when $n = 1$ the functions \bar{u} and \bar{v} decay exponentially. Cochran [13] showed that in this case

$$(\bar{u}', \bar{v}') = \bar{w}_\infty (\bar{u}, \bar{v}) \quad \text{as} \quad \eta \rightarrow \infty, \quad (12)$$

where $w_\infty = -2 \int_0^\infty \bar{u} d\eta$.

Numerical solutions of 9a, 9b and 9c subject to (10a) and (10b) are presented in Table 1 and Fig. 1. These results were obtained using a fourth-order Runge–Kutta quadrature routine twinned

with a Newton iteration scheme to determine the values of the unknowns $\bar{u}'(0) = \bar{u}_0$ and $\bar{v}'(0) = \bar{v}_0$. As is to be expected our results are in complete agreement with Denier and Hewitt [12], however, here we also present values for \bar{u}_0 and \bar{v}_0 for each value of n . For the case when $n = 1$ our results are in agreement with those presented by Healey [14].

3. The inviscid stability problem

The governing Eqs. (1) and (2) in component form are

$$\frac{1}{r} \frac{\partial}{\partial r}(ru) + \frac{1}{r} \frac{\partial v}{\partial \theta} + \frac{\partial w}{\partial z} = 0, \tag{13a}$$

$$u \frac{\partial u}{\partial r} + \frac{v}{r} \frac{\partial u}{\partial \theta} + w \frac{\partial u}{\partial z} - \frac{(v+r)^2}{r} = -\frac{\partial p}{\partial r} + \frac{1}{Re} \left[\frac{\partial}{\partial z} \left(\mu \frac{\partial u}{\partial z} \right) + \mathcal{L}_r \right], \tag{13b}$$

$$u \frac{\partial v}{\partial r} + \frac{v}{r} \frac{\partial v}{\partial \theta} + w \frac{\partial v}{\partial z} + \frac{uv}{r} + 2u = -\frac{1}{r} \frac{\partial p}{\partial \theta} + \frac{1}{Re} \left[\frac{\partial}{\partial z} \left(\mu \frac{\partial v}{\partial z} \right) + \mathcal{L}_\theta \right], \tag{13c}$$

Table 1

Numerical values of the basic flow parameters for $n = 1, 0.9, 0.8, 0.7, 0.6$. For $n = 1$ the value of η_∞ represents the dimensionless distance away from the disk at which the solutions have sufficiently converged to their respective limiting values, as in this case the asymptotic boundary condition (12) has no specific dependence on η .

n	\bar{u}_0	$-\bar{v}_0$	η_∞	$-\bar{w}(\eta_\infty)$
1	0.5102	0.6159	20	0.8845
0.9	0.5069	0.6243	55	0.9698
0.8	0.5039	0.6362	100	1.0957
0.7	0.5017	0.6532	175	1.3051
0.6	0.5005	0.6778	645	1.7329

$$u \frac{\partial w}{\partial r} + \frac{v}{r} \frac{\partial w}{\partial \theta} + w \frac{\partial w}{\partial z} = -\frac{\partial p}{\partial z} + \frac{1}{Re} (\mathcal{L}_z), \tag{13d}$$

where

$$\mu = \left[\left(\frac{\partial u}{\partial z} \right)^2 + \left(\frac{\partial v}{\partial z} \right)^2 + \mathcal{L}_\mu \right]^{(n-1)/2}. \tag{13e}$$

Here the additional viscous terms $\mathcal{L}_r, \mathcal{L}_\theta, \mathcal{L}_z$ and \mathcal{L}_μ have been omitted as these terms will not appear in the upcoming analysis. The form of these additional terms is given in Appendix A.

We now perturb the basic flow solutions by writing $\mathbf{u} = \mathbf{u}_B + \mathbf{U}$. Substitution into (13a)–(13d) and (13e) and neglecting the nonlinear terms gives the linear disturbance equations

$$\frac{1}{r} \frac{\partial}{\partial r}(rU) + \frac{1}{r} \frac{\partial V}{\partial \theta} + \frac{\partial W}{\partial z} = 0, \tag{14}$$

$$r\bar{u} \frac{\partial U}{\partial r} + \bar{v} \frac{\partial U}{\partial \theta} + r^{(n-1)/(n+1)} Re^{-1/(n+1)} \bar{w} \frac{\partial U}{\partial z} + rU \frac{\partial \bar{u}}{\partial r} + \bar{u}U - 2(\bar{v}+1)V + rW \frac{\partial \bar{u}}{\partial z} = -\frac{\partial P}{\partial r} + r^{n-1} Re^{-1} \frac{\partial}{\partial z} \left(\bar{\mu} \frac{\partial U}{\partial z} + \bar{\bar{\mu}} \frac{\partial \bar{u}}{\partial z} \right), \tag{15}$$

$$r\bar{u} \frac{\partial V}{\partial r} + \bar{v} \frac{\partial V}{\partial \theta} + r^{(n-1)/(n+1)} Re^{-1/(n+1)} \bar{w} \frac{\partial V}{\partial z} + rU \frac{\partial \bar{v}}{\partial r} + \bar{u}V + 2(\bar{v}+1)U + rW \frac{\partial \bar{v}}{\partial z} = -\frac{1}{r} \frac{\partial P}{\partial \theta} + r^{n-1} Re^{-1} \frac{\partial}{\partial z} \left(\bar{\mu} \frac{\partial V}{\partial z} + \bar{\bar{\mu}} \frac{\partial \bar{v}}{\partial z} \right), \tag{16}$$

$$r\bar{u} \frac{\partial W}{\partial r} + \bar{v} \frac{\partial W}{\partial \theta} + r^{(n-1)/(n+1)} Re^{-1/(n+1)} \bar{w} \frac{\partial W}{\partial z} + U \left\{ \bar{w} \frac{\partial W}{\partial z} + U \left[\frac{\bar{w}(n-1)}{r(n+1)} + \frac{\partial \bar{w}}{\partial r} \right] + W \frac{\partial \bar{w}}{\partial z} \right\} = -\frac{\partial P}{\partial z}, \tag{17}$$

where P is the non-dimensional pressure perturbation and

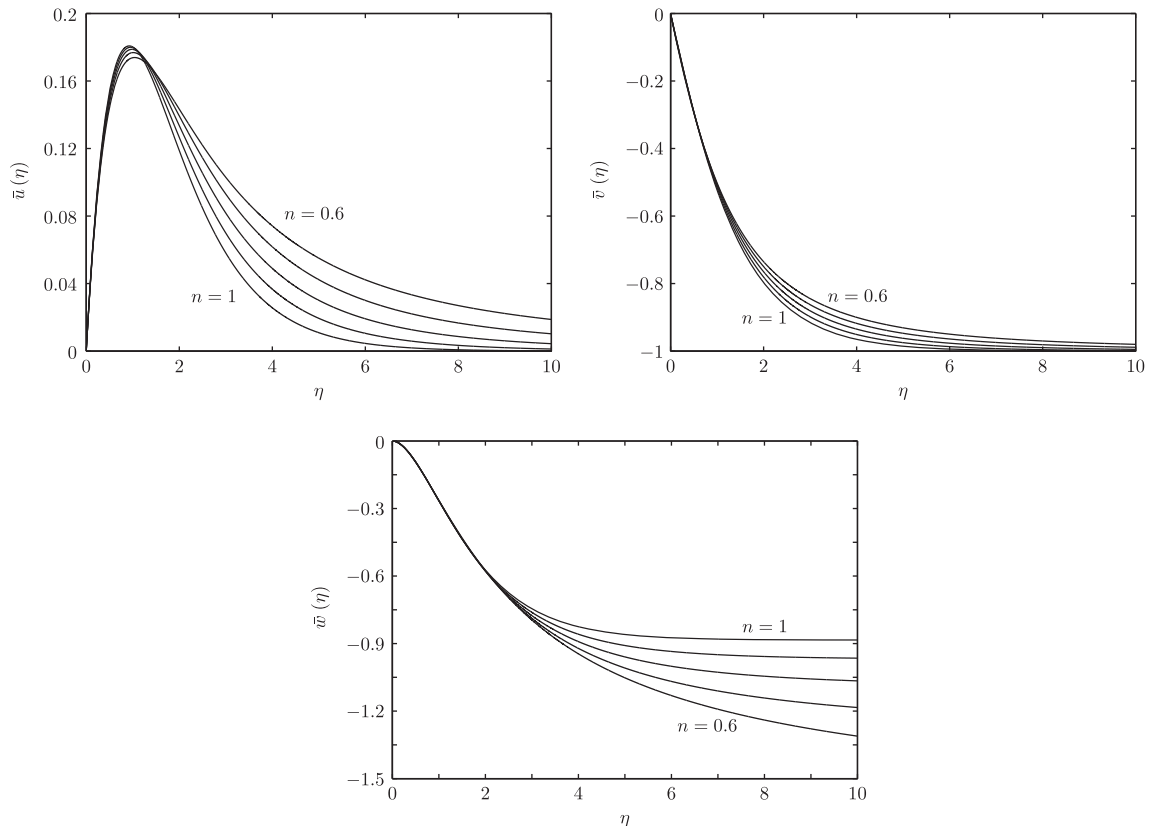


Fig. 1. Plots of \bar{u} , \bar{v} and \bar{w} versus η for $n = 1, 0.9, 0.8, 0.7, 0.6$. The η -axis has been truncated at $\eta = 10$. The value of η_∞ employed for each calculation is given in Table 1.

$$\bar{\mu} = \left[\left(\frac{\partial \bar{u}}{\partial z} \right)^2 + \left(\frac{\partial \bar{v}}{\partial z} \right)^2 \right]^{(n-1)/2}, \tag{18}$$

$$\bar{\mu} = (n-1) \left(\frac{\partial \bar{u}}{\partial z} \frac{\partial U}{\partial z} + \frac{\partial \bar{v}}{\partial z} \frac{\partial V}{\partial z} \right) \left[\left(\frac{\partial \bar{u}}{\partial z} \right)^2 + \left(\frac{\partial \bar{v}}{\partial z} \right)^2 \right]^{(n-3)/2}. \tag{19}$$

Following Hall [5], we consider disturbances to the basic flow proportional to

$$E = \exp \left[\frac{i}{\varepsilon^3} \left(\int^r \alpha(r, \varepsilon) dr + \theta \beta(\varepsilon) \right) \right], \tag{20}$$

where $\varepsilon = Re^{-1/[3(n+1)]}$. Hence, we have that $U = u(r, z)E$ and similarly for V, W and P . We note the inclusion of the ε^{-3} term as we expect from Gregory et al. [4] that these modes will have wavelengths scaled on the boundary layer thickness. Here $\alpha = \alpha_0 + \varepsilon \alpha_1 + \dots$ and $\beta = \beta_0 + \varepsilon \beta_1 + \dots$ are the wavenumbers in the \hat{r} and $\hat{\theta}$ directions, respectively.

The inviscid zone occupies the entirety of the boundary layer. The boundary layer thickness is given by $\delta = Re^{1/(n+1)}$, hence, the inviscid zone has thickness $O(\varepsilon^3)$. Here the velocities and pressure expand as

$$u = u_0(\eta) + \varepsilon u_1(\eta) + \dots, \tag{21a}$$

$$v = v_0(\eta) + \varepsilon v_1(\eta) + \dots, \tag{21b}$$

$$w = w_0(\eta) + \varepsilon w_1(\eta) + \dots, \tag{21c}$$

$$p = p_0(\eta) + \varepsilon p_1(\eta) + \dots. \tag{21d}$$

The expansions are then substituted into (14)–(17) along with (18) and (19), with the following forms for the differential operators for the disturbance terms

$$\frac{\partial}{\partial r} = \frac{\eta(1-n)}{r(n+1)} \frac{\partial}{\partial \eta} + \left(\frac{i}{\varepsilon^3} \right) (\alpha_0 + \varepsilon \alpha_1 + \dots), \quad \frac{\partial}{\partial \theta} = \left(\frac{i}{\varepsilon^3} \right) (\beta_0 + \varepsilon \beta_1 + \dots).$$

Equating terms of order ε^{-3} , we obtain

$$i\alpha_0 u_0 + \frac{i\beta_0 v_0}{r} + r^{(1-n)/(n+1)} w_0' = 0, \tag{22a}$$

$$i\bar{u} u_0 + r^{2/(n+1)} w_0 u' + i\alpha_0 p_0 = 0, \tag{22b}$$

$$i\bar{u} v_0 + r^{2/(n+1)} w_0 v' + \frac{i\beta_0 p_0}{r} = 0, \tag{22c}$$

$$i\bar{u} w_0 + r^{(1-n)/(n+1)} p_0' = 0, \tag{22d}$$

where the primes denote differentiation with respect to η and $\bar{u} = \alpha_0 \bar{u}r + \beta_0 \bar{v}$. Manipulation of the above gives the Rayleigh equation for w_0 , namely

$$\bar{u} (w_0'' - \kappa_0^2 w_0) - \bar{u}'' w_0 = 0, \tag{23}$$

where $\kappa_0^2 = r^{2(n-1)/(n+1)} (\alpha_0^2 + \beta_0^2/r^2)$ is the effective wavenumber and \bar{u} is the effective two-dimensional velocity profile. We are interested in the stationary modes so following Hall [5] we choose $\lambda_0 = \alpha_0 r/\beta_0$ such that

$$\bar{u} = \bar{u}'' = 0 \quad \text{at} \quad \eta = \bar{\eta}, \tag{24}$$

ensuring that (23) is not singular at $\eta = \bar{\eta}$. Rayleigh's equation is then solved subject to

$$w_0 = 0 \quad \text{at} \quad \eta = 0 \quad \text{and} \quad w_0 \rightarrow 0 \quad \text{as} \quad \eta \rightarrow \infty. \tag{25}$$

The eigenvalue problem for κ_0 was solved using central differences for a range of values of n . The results are presented in Table 2 and have been plotted in Fig. 2. Here the solution for w_0 has been normalised with $w_0' = 1$ at $\eta = 0$. Since we have that

$$\tan \left(\frac{\pi}{2} - \phi \right) = \frac{\alpha r}{\beta}, \tag{26}$$

Table 2
Numerical values for $\lambda_0, \bar{\eta}, \kappa_0$ and ϕ_0 for $n = 1, 0.9, 0.8, 0.7, 0.6$.

n	λ_0	$\bar{\eta}$	κ_0	ϕ_0 (°)
1	4.256	1.458	1.162	13.22
0.9	4.086	1.455	1.149	13.75
0.8	3.926	1.445	1.143	14.29
0.7	3.782	1.423	1.144	14.81
0.6	3.663	1.388	1.157	15.27

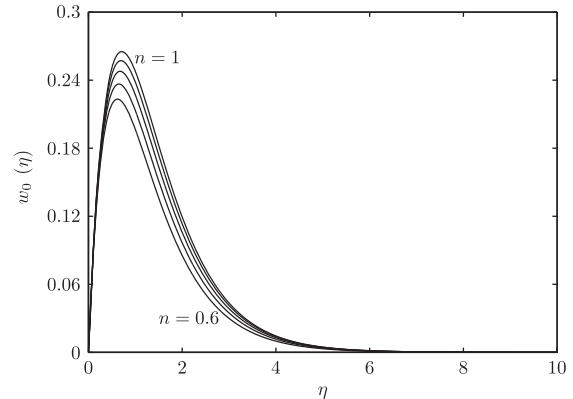


Fig. 2. The inviscid motion eigenfunction $w_0(\eta)$ for $n = 1, 0.9, 0.8, 0.7, 0.6$.

the leading order approximations to the wave angle, ϕ_0 , for each value of n can also be calculated. Again the results are presented in Table 2.

The corrections to the effective wavenumber and wave angle ϕ of the disturbance may be determined by considering the next order solutions in the inviscid layer. It is found that w_1 satisfies

$$\bar{u} (w_1'' - \kappa_0^2 w_1) - \bar{u}'' w_1 = 2\bar{u} r^{2(n-1)/(n+1)} \left(\alpha_0 \alpha_1 + \frac{\beta_0 \beta_1}{r^2} \right) w_0 + r \left(\alpha_1 - \frac{\alpha_0 \beta_1}{\beta_0} \right) \left(\bar{u}'' - \frac{\bar{u} \bar{u}''}{\bar{u}} \right) w_0. \tag{27}$$

The second term on the right-hand side of (27) causes w_1 to have a logarithmic singularity at $\eta = \bar{\eta}$, where $\bar{u} = 0$. This can be removed by introducing a critical layer at $\eta = \bar{\eta}$. The solution for w_1 for $\eta > \bar{\eta}$ is then

$$w_1 = 2r^{2(n-1)/(n+1)} \left(\alpha_0 \alpha_1 + \frac{\beta_0 \beta_1}{r^2} \right) w_0(\eta) \int_{\bar{\eta}}^{\eta} \frac{d\zeta}{w_0^2(\zeta)} \times \int_{\infty}^{\zeta} w_0^2(\theta) d\theta + r \left(\alpha_1 - \frac{\alpha_0 \beta_1}{\beta_0} \right) w_0(\eta) \int_{\bar{\eta}}^{\eta} \frac{d\zeta}{w_0^2(\zeta)} \times \int_{\infty}^{\zeta} w_0^2(\theta) \left[\frac{\bar{u}''(\theta) \bar{u}(\theta) - \bar{u}(\theta) \bar{u}''(\theta)}{\bar{u}^2(\theta)} \right] d\theta, \tag{28}$$

where $\bar{\eta} > \bar{\eta}$. For $\eta < \bar{\eta}$ the path of integration is deformed above the singularity in the complex plane since $\bar{u}'(\bar{\eta}) < 0$. Gajjar [15] presents a linear critical layer analysis in the Newtonian case, showing that for flows such as this with $\bar{u}'(\bar{\eta}) < 0$ the path of integration must be deformed above the singularity in order to match the flow in the inviscid layer.

The solutions in the inviscid layer do not satisfy the boundary conditions at $\eta = 0$, so we require a wall layer of thickness $O(\varepsilon^4)$. Let us define the wall layer coordinate ζ by $\zeta = r^{(1-n)/(n+1)} Re^{4/[3(n+1)]} z$ then the basic flow component \bar{u} expands as

$$\bar{u} = \eta \bar{u}_0 + \dots = \varepsilon \zeta \bar{u}_0 + \dots,$$

with similar expansions for \bar{v} and \bar{w} . Inside the wall layer the disturbance velocities and pressure are given by

Table 3
Numerical values of the integrals I_1 and I_2 for $n = 1, 0.9, 0.8, 0.7, 0.6$.

n	I_1	I_2
1	0.0911	0.0592 + 0.0299i
0.9	0.0848	0.0619 + 0.0291i
0.8	0.0774	0.0653 + 0.0281i
0.7	0.0689	0.0671 + 0.0270i
0.6	0.0594	0.0691 + 0.0255i

Table 4
First order corrections to the effective wavenumber and wave angle for $n = 1, 0.9, 0.8, 0.7, 0.6$.

n	$-\kappa_1$	λ_1
1	9.14	17.43
0.9	10.18	17.66
0.8	11.58	17.97
0.7	13.16	18.20
0.6	15.34	18.59

$$u = U_0(\xi) + \varepsilon U_1(\xi) + \dots, \tag{29a}$$

$$v = V_0(\xi) + \varepsilon V_1(\xi) + \dots, \tag{29b}$$

$$w = \varepsilon W_0(\xi) + \varepsilon^2 W_1(\xi) + \dots, \tag{29c}$$

$$p = \varepsilon P_0(\xi) + \varepsilon^2 P_1(\xi) + \dots \tag{29d}$$

Despite the appearance of additional viscous terms in the leading order governing equations for a power-law fluid, analytic solutions are obtainable. The leading order solutions are given in terms of the Airy function $\text{Ai}(\gamma\xi)$, where $\gamma = (i\bar{u}_0/n\bar{\mu}_0)^{1/3}$ with $\bar{u}_0 = \alpha_0\bar{u}_0r + \beta_0\bar{v}_0$ and $\bar{\mu}_0 = [\bar{u}_0^2 + \bar{v}_0^{2(n-1)/2}]^{1/2}$. For large ξ we find that

$$W_0 \approx w'_0(0)\xi + \frac{w'_0(0)\text{Ai}'(0)}{\gamma \int_0^\infty \text{Ai}(s) ds}. \tag{30}$$

This provides the matching condition for w_1 , namely

$$w_1 \rightarrow \frac{w'_0(0)\text{Ai}'(0)}{\gamma \int_0^\infty \text{Ai}(s) ds} \text{ as } \eta \rightarrow 0. \tag{31}$$

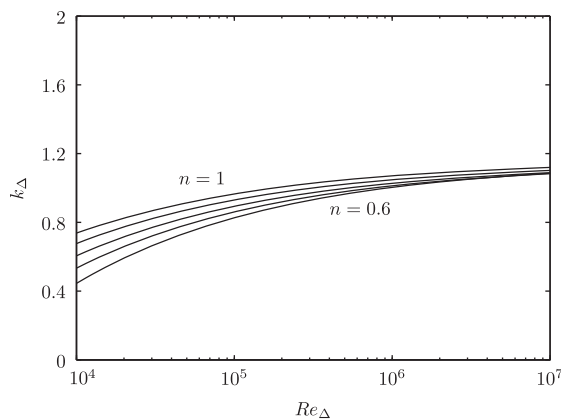
Thus, from (28) we obtain the linear eigenrelation

$$\frac{[w'_0(0)]^2 \text{Ai}'(0)}{\gamma \int_0^\infty \text{Ai}(s) ds} = 2r^{2(n-1)/(n+1)} \left(\alpha_0\alpha_1 + \frac{\beta_0\beta_1}{r^2} \right) I_1 + \left(\frac{\alpha_1}{\beta_0} - \frac{\alpha_0\beta_1}{\beta_0^2} \right) rI_2. \tag{32}$$

Here

$$I_1 = \int_0^\infty w_0^2(\theta) d\theta,$$

$$I_2 = \beta_0 \int_0^\infty w_0^2(\theta) \left[\frac{\bar{u}''(\theta)\bar{u}(\theta) - \bar{u}(\theta)\bar{u}''(\theta)}{\bar{u}^2(\theta)} \right] d\theta.$$



Our calculations for I_1 and I_2 are presented in Table 3. Using the well known values for $\text{Ai}'(0)$ and $\int_0^\infty \text{Ai}(s) ds$, we are able to solve the eigenrelation (32) giving

$$\left(\alpha_0\alpha_1 + \frac{\beta_0\beta_1}{r^2} \right) r^{2(n-1)/(n+1)} = \kappa_1 r^{-2/[3(n+1)]} \kappa_0, \tag{33a}$$

$$\left(\frac{\alpha_1}{\beta_0} - \frac{\alpha_0\beta_1}{\beta_0^2} \right) r = \lambda_1 r^{-2/[3(n+1)]}, \tag{33b}$$

where κ_1 and λ_1 are constants that are determined during the solution process. Numerical values for κ_1 and λ_1 are presented in Table 4 for a range of values of n . Our results, in the Newtonian case, are in good agreement with those of Gajjar [15].

By introducing the modified Reynolds number, $Re_\Delta = r^{2/(n+1)} Re^{1/(n+1)}$, based on the boundary layer thickness and the local azimuthal velocity of the disk we are able to formulate expressions for the local wavenumber and wave angle that have no explicit dependence on the radial variable r . Since we have that

$$k_\Delta = r^{(n-1)/(n+1)} \sqrt{\alpha^2 + \frac{\beta^2}{r^2}} = \kappa_0 + r^{2(n-1)/(n+1)} \left(\alpha_0\alpha_1 + \frac{\beta_0\beta_1}{r^2} \right) \frac{\varepsilon}{\kappa_0} + \dots,$$

$$\tan\left(\frac{\pi}{2} - \phi\right) = \lambda_0 + r \left(\frac{\alpha_1}{\beta_0} - \frac{\alpha_0\beta_1}{\beta_0^2} \right) \varepsilon + \dots,$$

where k_Δ is the local wavenumber, (33a) and (33b) give

$$k_\Delta = \kappa_0 + \kappa_1 Re_\Delta^{-1/3} + \dots, \tag{34a}$$

$$\tan\left(\frac{\pi}{2} - \phi\right) = \lambda_0 + \lambda_1 Re_\Delta^{-1/3} + \dots. \tag{34b}$$

Plots of k_Δ and ϕ for $Re \gg 1$, as functions of Re_Δ are presented in Fig. 3. In Fig. 3(a) and (b) the flow is unstable in the region below, and above, the curves, respectively. Thus, as n decreases the neutral values of the effective wavenumber of the disturbances decrease while the values of the wave angle increases.

4. Conclusion

We have shown that the inviscid stability analysis used to describe the upper-branch stationary neutral modes of the von Kármán flow (for $Re \gg 1$) can be extended to incorporate the rheology of a power-law fluid. The prediction for the angle of the spiral vortices resulting from the instability for the case when $n = 1$ agrees well with existing numerical and experimental results. The results from Fig. 3 show that at the same value of the modified Reynolds number the local neutral wavenumber will decrease with decreasing n and that the wave angle will increase with decreasing n . This suggests that shear-thinning fluids may have a stabilising effect on the inviscid flow as fewer spiral vortices with a greater

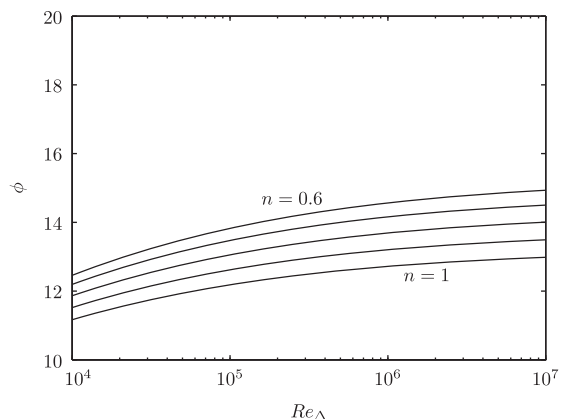


Fig. 3. Plots of the asymptotic neutral wavenumber k_Δ and wave angle ϕ predictions for $n = 1, 0.9, 0.8, 0.7$ and 0.6 using two terms of the asymptotic results.

wave angle are predicted as n decreases from 1. However, the stabilising or destabilising effect of the fluid index n in terms of the critical Reynolds number can only be determined by numerical solution of the full governing stability equations. In addition, the absolute instability must be considered to determine the effect on the global instability of such non-Newtonian flows. These investigations are outside the scope of the current study.

Besides the above directions, there are other areas for future work on this problem. The possibility of lower-branch stationary modes could be studied asymptotically, as in Hall [5] for the Newtonian flow problem. The results presented here could be reproduced for shear-thickening fluids since the asymptotic analysis holds for all $n > 0$, although as mentioned in Section 2 due care and attention needs to be given to the basic solutions in this case. Of particular interest would be numerical solutions of the governing stability equations to compare the asymptotic results (34). A numerical study will determine the effect of a shear-thinning fluid on the critical Reynolds number for the onset of linear instability. Our analysis predicts that co-rotating spiral vortices will occur for large enough Reynolds numbers.

The experimental studies of Nasr-El-Din et al. [16] into the effect of gelled acids on the erosion of calcite marble rotating disks may be relevant here. The gelled acids used were shear-thinning fluids with measured fluid index $0.55 < n < 0.70$. For sufficiently large rotation rates spiral patterns of erosion were observed on the disk, which reduced as n decreased. Of interest would be experiments at larger Reynolds number with which to compare our theoretical analysis.

Acknowledgments

PTG gratefully acknowledges the support of the Engineering and Physical Sciences Research Council UK for his PhD studies. SOS is especially thankful to the School of Mathematics and Statistics, University of Western Australia, for funding and hospitality during her visit there, where some of the research was carried out.

Appendix A. Additional viscous terms

The additional viscous terms omitted from the analysis in Section 3 are presented here, for completeness.

$$\mathcal{L}_r = \frac{2}{r} \frac{\partial}{\partial r} \left(\mu r \frac{\partial u}{\partial r} \right) + \frac{1}{r} \frac{\partial}{\partial \theta} \left\{ \mu \left[r \frac{\partial}{\partial r} \left(\frac{v}{r} \right) + \frac{1}{r} \frac{\partial u}{\partial \theta} \right] \right\} + \frac{\partial}{\partial z} \left(\mu \frac{\partial w}{\partial r} \right) - \frac{2\mu}{r^2} \left(\frac{\partial v}{\partial \theta} + u \right), \quad (\text{A.1})$$

$$\mathcal{L}_\theta = \frac{1}{r^2} \frac{\partial}{\partial r} \left\{ \mu \left[r^3 \frac{\partial}{\partial r} \left(\frac{v}{r} \right) + r \frac{\partial u}{\partial \theta} \right] \right\} + \frac{2}{r} \frac{\partial}{\partial \theta} \left[\mu \left(\frac{1}{r} \frac{\partial v}{\partial \theta} + \frac{u}{r} \right) \right] + \frac{\partial}{\partial z} \left(\mu \frac{\partial w}{r \partial \theta} \right), \quad (\text{A.2})$$

$$\mathcal{L}_z = \frac{1}{r} \frac{\partial}{\partial r} \left[\mu r \left(\frac{\partial u}{\partial z} + \frac{\partial w}{\partial r} \right) \right] + \frac{1}{r} \frac{\partial}{\partial \theta} \left[\mu \left(\frac{\partial v}{\partial z} + \frac{1}{r} \frac{\partial w}{\partial \theta} \right) \right] + 2 \frac{\partial}{\partial z} \left(\mu \frac{\partial w}{\partial z} \right), \quad (\text{A.3})$$

$$\mathcal{L}_\mu = 2 \left(\frac{\partial u}{\partial r} \right)^2 + 2 \left(\frac{1}{r} \frac{\partial v}{\partial \theta} + \frac{u}{r} \right)^2 + 2 \left(\frac{\partial w}{\partial z} \right)^2 + \left[r \frac{\partial}{\partial r} \left(\frac{v}{r} \right) + \frac{1}{r} \frac{\partial u}{\partial \theta} \right]^2 + 2 \frac{\partial u}{\partial z} \frac{\partial w}{\partial r} + \left(\frac{\partial w}{\partial r} \right)^2 + \frac{2}{r} \frac{\partial v}{\partial z} \frac{\partial w}{\partial \theta} + \left(\frac{1}{r} \frac{\partial w}{\partial \theta} \right)^2. \quad (\text{A.4})$$

References

- [1] T. von Kármán, Über laminare und turbulente Reibung, *Z. Angew. Math. Mech.* 1 (1921) 233–252.
- [2] G.K. Batchelor, Note on the class of solutions of the Navier-Stokes equations representing steady non-rotationally symmetric flow, *Q. J. Mech. Appl. Math.* 4 (1951) 29–41.
- [3] U.T. Bödewadt, Die Drehströmung über festem Grund, *Z. Angew. Math. Mech.* 20 (1940) 241–252.
- [4] N. Gregory, J.T. Stuart, W.S. Walker, On the stability of three-dimensional boundary layers with applications to the flow due to a rotating disk, *Phil. Trans. R. Soc. Lond. A* 248 (1955) 155–199.
- [5] P. Hall, An asymptotic investigation of the stationary modes of instability of the boundary layer on a rotating disc, *Proc. R. Soc. Lond. A* 406 (1986) 93–106.
- [6] M.R. Malik, The neutral curve for stationary disturbances in rotating-disk flow, *J. Fluid Mech.* 164 (1986) 275–287.
- [7] R.J. Lingwood, Absolute instability of the Ekman layer and related rotating flows, *J. Fluid Mech.* 331 (1997) 405–428.
- [8] C. Davies, P.W. Carpenter, Global behaviour corresponding to the absolute instability of the rotating-disc boundary layer, *J. Fluid Mech.* 486 (2003) 287–329.
- [9] P. Mitschka, Nicht-Newtonische Flüssigkeiten II. Drehströmungen Ostwald-de Waelescher Nicht-Newtonische Flüssigkeiten, *Collect. Czech. Chem. Commun.* 29 (1964) 2892–2905.
- [10] P. Mitschka, J. Ulbrecht, Nicht-Newtonische Flüssigkeiten IV. Strömung Nicht-Newtonische Flüssigkeiten Ostwald-de Waelescher Typs in der Umgebung Rotierender Drehkegel und Schieben, *Collect. Czech. Chem. Commun.* 30 (1965) 2511–2526.
- [11] H.I. Andersson, E. de Korte, R. Meland, Flow of a power-law fluid over a rotating disk revisited, *Fluid Dyn. Res.* 28 (2001) 75–88.
- [12] J.P. Denier, R.E. Hewitt, Asymptotic matching constraints for a boundary-layer flow of a power-law fluid, *J. Fluid Mech.* 518 (2004) 261–279.
- [13] W.G. Cochran, The flow due to a rotating disk, *Proc. Camb. Phil. Soc.* 30 (1934) 365–375.
- [14] J.J. Healey, Inviscid long-wave theory for the absolute instability of the rotating-disc boundary layer, *Proc. R. Soc. Lond. A* 462 (2006) 1467–1492.
- [15] J.S.B. Gajjar, Nonlinear critical layers in the boundary layer on a rotating disk, *J. Eng. Math.* 57 (2007) 205–217.
- [16] H.A. Nasr-El-Din, A.M. Al-Mohammad, A.M. Al-Aamri, O. Al-Fuwaires, Reaction kinetics of gelled acids with calcite, *SPEPO* 23 (3) (2008) 353–361.